A novel missense *TUBB4B* variant outside of the canonical hotspot is associated with cone-rod dystrophy and sensorineural hearing loss.

Lauren Y. Cao,¹ Anna Duemler,¹ Emily H. Jung,¹ Ramiro S. Maldonado,¹ Sarah Richards,² Elena R. Schiff,^{3,4} Omar A. Mahroo,^{3,4} Andrew R. Webster,^{3,4} Siying Lin,^{5,6,7} Beau J. Fenner,^{8,9} Alessandro lannaccone,^{1,10,11} Oleg Alekseev¹

- ² Publications and Collaborations, GeneDx, LLC, Gaithersburg, Maryland, USA
- ³ NIHR Biomedical Research Centre, Moorfields Eye Hospital and the UCL Institute of Ophthalmology, London, UK
- ⁴ Institute of Ophthalmology, University College London, UK
- ⁵ Division of Evolution, Infection and Genomics, School of Biological Sciences, Faculty of Biology, Medicine and Health, University of Manchester, Manchester, UK
- ⁶ Manchester Centre for Genomic Medicine, Saint Mary's Hospital & Department of Ophthalmology, Manchester Royal Eye Hospital, Manchester University NHS Foundation Trust, Manchester, UK
- ⁷ National Institute of Health Research Biomedical Research Centre at Moorfields Eye Hospital and the UCL Institute of Ophthalmology, London, UK
- ⁸ Department of Medical Retina, Singapore National Eye Centre, Singapore
- ⁹ Ocular Genetics, Singapore Eye Research Institute, Singapore
- ¹⁰ Current affiliation: Cell and Gene Therapy, Biopharma and Ophthalmology Division, Astellas Pharmaceuticals US, Inc., Northbrook, Illinois, USA
- ¹¹ Current affiliation: Department of Ophthalmology, University of North Carolina School of Medicine, Chapel Hill, North Carolina, USA

¹ Department of Ophthalmology, Duke University School of Medicine, Durham, North Carolina, USA

Corresponding author:

Oleg Alekseev, MD, PhD

Department of Ophthalmology

Duke University School of Medicine

Phone 919.613.7584

Fax 919.681.6474

oleg.alekseev@duke.edu

ABSTRACT

Introduction

Pathogenic variants in *TUBB4B*, which encodes the β-tubulin 4B isotype of microtubule subunits, have been associated with Leber congenital amaurosis with early-onset deafness (LCAEOD), an autosomal dominant condition characterized by early and severe loss of photoreceptor and cochlear cells. The majority of reported cases feature early disease onset and are caused by missense mutations in the R390/R391 hotspot.

Methods

Multimodal evaluation included ultra-widefield pseudocolor and autofluorescence fundus photography, spectral-domain optical coherence tomography, full-field electroretinography, Goldmann kinetic perimetry, audiography, and genetic testing with next-generation sequencing.

Results

We report seven individuals from three unrelated families affected by cone-rod dystrophy and sensorineural hearing loss associated with a novel variant in *TUBB4B* (c.784C>T, p.R262W). Cone-rod dystrophy associated with this variant generally features a later age of onset compared to the Leber congenital amaurosis caused by variants in the canonical hotspot.

Discussion

This report expands the mutation spectrum and phenotypic range of *TUBB4B*-associated retinopathies beyond the R390/R391 hotspot and may offer insight into the pathogenesis of this rare tubulinopathy.

Keywords

TUBB4B, LCAEOD, β-tubulin 4B, cone-rod dystrophy

INTRODUCTION

Microtubules participate in vital cell processes, such as cell division, locomotion, intracellular transport, and formation and maintenance of cilia. In primary cilia, nine double-microtubules arranged in a ring give rise to a structure called the axoneme, which supports the cilium and acts as a scaffold for protein complexes ¹. Photoreceptor cells are specialized primary cilia composed of hundreds of light-sensitive membrane discs stacked along the axoneme. Such anatomical organization allows for high efficiency of visual transduction but requires transport of essential proteins and waste products, which is facilitated by the axoneme ². Microtubules within the axoneme interact with a vast array of microtubule-associated proteins, including kinesin, a motor protein responsible for anterograde transport ³.

Although they appear deceptively uniform at the macromolecular level, microtubules are highly diverse at the functional level due to two main factors: differences in tubulin isotypes and post-translational modifications 4 . Humans have a diverse set of nine α - and nine β -tubulin isotypes, which allow for variability in microtubule dynamics and mechanics, as well as recruitment and activity of microtubule-associated proteins. α - and β -tubulin isotypes are highly conserved, most of them distinguished primarily by a variable region of around 15-20 amino acids near the C-terminus, which is thought to play a role in microtubule assembly 5 .

Mutations in tubulin genes cause an extensive and complex set of sensorineural disorders collectively known as tubulinopathies. Whereas most tubulinopathies are commonly characterized by severe brain malformations ⁶, mutations in *TUBB4B*, which encodes β-tubulin 4B, have been reported to cause Leber congenital amaurosis with early onset deafness (LCAEOD), a condition that affects photoreceptors and cochlear cells ⁷⁻¹². Leber congenital amaurosis (LCA) is a clinically and genetically heterogeneous disorder characterized by early and severe retinal degeneration. LCAEOD is an autosomal dominant condition that combines the retinal phenotype of LCA with sensorineural hearing loss (SNHL) as early as the first decade of life ^{9, 10}.

Notably, the majority of currently published cases of *TUBB4B*-associated LCAEOD are caused by mutations in residues R390/R391 $^{9-14}$. These residues are thought to play a crucial role in α - and β -tubulin interactions, impairment of which leads to reduced microtubule growth rates 10 . In contrast to previous reports, we describe a novel *TUBB4B* variant c.784C>T (p.R262W) identified in seven individuals from three unrelated families with cone-rod dystrophy and sensorineural hearing loss. This residue is located in the kinesin-binding domain of β -tubulin and is thought to compromise intracellular anterograde protein transport through the impairment of microtubule-kinesin interactions 15 . This finding expands the mutation spectrum of *TUBB4B*-associated retinopathies beyond the R390/R391 hotspot and broadens their range of clinical manifestation beyond the early-onset phenotype of LCA.

METHODS

Multimodal patient evaluation

All patient data were obtained in compliance with the approved Institutional Review
Board protocols of the Duke University Health System, Moorfields Eye Hospital, and the
Singapore National Eye Center. Best-corrected visual acuity (BCVA) was measured using the
Early Treatment Diabetic Retinopathy Study (ETDRS) retro-illuminated cabinet (Precision
Vision, Woodstock, IL). Fundus pseudocolor and autofluorescence (FAF) ultra-widefield images
were obtained using the Optos California device (Marlborough, MA, and Dunfermline, UK).
Macular spectral domain optical coherence tomography (SD-OCT) scans were obtained using
the Heidelberg Spectralis imaging platform (Heidelberg, Germany). Full-field electroretinography
(ERG) was performed with the Diagnosys ColorDome equipped with E³ console and Espion
software (Lowell, MA) following the International Society for Clinical Electrophysiology of Vision
(ISCEV) Standard. Goldmann kinetic perimetry was assessed with the Haag-Streit Octopus 900
Pro System (Köniz, Switzerland). Audiography was performed using conventional methodology
with the GSI 61 audiometer (patients III1 and III3) or GSI AudioStarPro audiometer (patients I1,

II1, and III2) (Grason-Stadler, Eden Praire, MN) equipped with ER-3A inserts (patients I1, III2, and III3) or TDH-50 phones (patients II1 and III1).

Genetic testing

Genetic testing of Family A was performed by the GeneDx laboratory (Gaithersburg, MD). Using genomic DNA from AIII2, her mother AII1, and maternal grandmother AI2 as a trio exome sequencing (ES), and separately as a singleton ES for AIII3, the exonic regions and flanking splice junctions of the genome were captured using the IDT xGen Exome Research Panel v1.0 (Integrated DNA Technologies, Coralville, IA). Massively parallel (NextGen) sequencing was done on an Illumina system with 100 bp or greater paired-end reads. Reads were aligned to human genome build GRCh37/UCSC hg19 and analyzed for sequence variants using a custom-developed analysis tool. Targeted sequencing was used to confirm the presence of variant in III1. In brief, genomic DNA from patient AIII1 was used to PCR-amplify the relevant portion of the *TUBB4B* gene, and capillary sequencing was performed. Bi-directional sequence was assembled, aligned to reference gene sequences based on human genome build GRCh37/UCSC hg19, and analyzed for the presence of the c.784C>T variant. Additional sequencing technology and variant interpretation protocol has been previously described ¹⁶. Individuals AI1, AI3, AII2, and AIII4 were unavailable for genetic testing.

Genetic testing of Family B was performed by the UK NHS Genomic Medicine Service. Whole genome sequencing (WGS) was carried out, and data were analyzed using virtual PanelApp panels ¹⁷ for Retinal disorders (v2.195) and Hearing loss (v2.5).

Genetic testing of Family C was performed by the Molecular Vision Laboratory (Hillsboro, OR) using the Vision Panel (v21.2), which consists of 1,211 genes, the mitochondrial genome, and mitochondrial nuclear genes. Direct testing for pathogenic variants was performed by target enrichment and Next Generation Sequencing. Identified pertinent pathogenic variants were confirmed by Sanger sequencing. All exons and exon/intron boundaries were sequenced. Alignment and variant calling were done using GRCh37.

Bioinformatics analyses

Single-cell RNA sequencing analysis of β -tubulin isotypes in human ocular tissues was generated by Spectacle (https://singlecell-eye.org) based on the integrated lowa dataset. Protein ribbon structures of tubulin β -4B chain were generated by AlphaFold3 ¹⁸.

PRESENTATION OF CASES

Family A

The proband (Al2) is a 65-year-old African American female, who was referred to the Duke Eye Center for evaluation of suspected Usher syndrome (see pedigree in Fig. 1A). She had experienced post-lingual hearing loss and received cochlear implants at age 15. Audiography at age 46 showed moderate to severe bilaterally symmetrical SNHL (Fig. S1) with 84% speech discrimination and normal tympanometry. By age 30 she could no longer read or write due to vision loss. Her medical history also included sick sinus syndrome with pacemaker placement, coronary artery disease, hypothyroidism, and microcytic anemia. Her BCVA was no light perception in each eye. Slit lamp biomicroscopy examination of the anterior segment was unremarkable. Dilated fundus examination demonstrated marked optic disc pallor, macular atrophy, nummular pigment deposits in the macula and periphery, and severe vascular attenuation and sheathing of both eyes (Fig. 2A). FAF imaging revealed extensive hypoautofluorescence in the posterior pole and mid-periphery of both eyes (Fig. 2B). Macular SD-OCT scans showed severe loss of the outer retinal layers bilaterally with abundant intraand subretinal hyperreflective material (SHRM) in part due to macular pigmentary deposits and disseminated hypertransmission defects (HTDs) due to the retinal pigment epithelium (RPE) loss noted already on FAF imaging (Fig. 2C). Optic nerve OCT showed marked attenuation of the retinal nerve fiber layer and the ganglion cell layer.

The proband's elder daughter (All1) is a 48-year-old female with history of childhoodonset post-lingual hearing loss, who had experienced nyctalopia since age 10 and photopsias since age 16. Audiography at age 40 showed moderate to severe bilaterally symmetrical SNHL (Fig. S1) with excellent word recognition and normal tympanometry. She developed light-aversion and visual field loss at age 29 and reduced central vision and dyschromatopsia at age 40. Her medical history was remarkable for hypothyroidism. Her BCVA was 4/200 in the right eye and 3/200 in the left eye. Findings from her fundus examination were similar to the proband's (Fig. 2A). FAF imaging showed disseminated peripheral nummular hypoautofluorescence due to both pigmentary changes and patches of RPE atrophy surrounding a pericentral ring of hyperautofluorescence and dense central hypoautofluorescence (Fig. 2B). Macular SD-OCT scans demonstrated generalized peripheral ellipsoid zone loss and retinal thinning, HTDs due to RPE atrophy, and parafoveal choroidal excavation with underlying breaks in the Bruch's membrane (Fig. 2C).

The proband's younger daughter (AII2), the half-sister of AII1, is a 45-year-old female with history of deafness and blindness. Although she was unavailable to undergo ophthalmic and audiological evaluations, she was reported by her family members to suffer from a similar condition affecting her vision and hearing from an early age.

The proband's elder grandson (AIII1), the son of AII1, is a 28-year-old male with history of early-onset post-lingual hearing loss, who developed nyctalopia at age 6. Audiography at age 5 showed mild to moderate SNHL (Fig. S1) and normal tympanometry bilaterally. He has recently been experiencing photopsias and difficulty reading small print. His medical history was notable for mitral regurgitation. His BCVA was 20/400 in each eye, and the pattern of fundus examination findings was similar to those of his mother (AII1) and grandmother (AI2) (Fig. 2A) yet significantly milder. Similar to the proband's elder relatives, dense macular hypoautofluorescence surrounded by a ring of hyperautofluorescence and an additional ring of speckled hypoautofluorescence at the arcades was seen on FAF imaging (Fig. 2B). Similar speckled hypoautofluorescence changes were also seen mid- and far-peripherally, without any nummular changes. Macular SD-OCT scans demonstrated similar outer retinal layer loss and

RPE atrophy, in addition to dense foveal SHRM centrally due to foveal pigment clumping (Fig. 2C). Initial choroidal excavation changes were also seen juxtafoveally in the right eye.

The proband's elder granddaughter (AIII2), a daughter of AII1, is a 25-year-old female with history of congenital nyctalopia, high myopia, and childhood-onset post-lingual hearing loss. Audiography at age 20 showed mild bilaterally symmetrical SNHL (Fig. S1) with excellent word recognition and normal tympanometry. Her medical history was notable for short stature, scoliosis, and dolichocephaly. Her BCVA was 20/800 eccentrically in the right eye and 20/320 in the left eye. Findings from her fundus examination (Fig. 2A) and macular SD-OCT (Fig. 2C) were similar to those previously described in her family. FAF imaging demonstrated disseminated peripheral speckled hypoautofluorescence with radially-oriented streaks of hypoautofluorescence throughout the periphery of both eyes, a hyperautofluorescent ring at and inside the arcades, as well as central dense hypoautofluorescence (Fig. 2B).

The proband's younger granddaughter (AIII3), a daughter of AII1, is a 22-year-old female with history of retinopathy of prematurity, nystagmus, ptosis, and childhood-onset post-lingual hearing loss. Audiogram at age 18 showed moderate bilaterally symmetrical SNHL (Fig. S1) with excellent word recognition and normal tympanometry. Her medical history also included short stature, scoliosis, seizures, periventricular leukomalacia, microcytic anemia, menorrhagia, and vitamin D insufficiency. Her BCVA was 20/160 in the right eye and 20/200 in the left eye. Findings of fundus examination and FAF imaging (Fig. 2) were all in line with those previously described in her family. FAF imaging was remarkable for the dense macular hypoautofluorescence seen in all other subjects, surrounded in this case by a very thin ring of perilesional hyperautofluorescence and a faint hyperautofluorescent halo along the arcades and around the disc. The midperiphery showed a diffuse reduction of the autofluorescence signal compared to the far periphery as well.

Given that patient AIII3 is the youngest of all affected family members, her evaluation provided an opportunity to characterize this condition prior to the onset of widespread retinal

dystrophy. Macular SD-OCT scans obtained at three-year intervals (15, 18, and 21 years of age) demonstrate the rate of progression of central macular outer retinal and RPE atrophy and development of SHRM (Fig. 3). Goldmann kinetic perimetry showed mild constriction of I3e and I4e isopters, with bilateral centro-cecal scotomas and enlarged blind spots but otherwise very well-preserved peripheral visual field limits (Fig. 4A). Full-field ERG revealed mildly reduced scotopic and moderately reduced and delayed photopic responses (Fig. 4B), with the reduction of cone-mediated responses being clearly out of proportion to the relatively small area of central ellipsoid zone loss. Overall, the ERG recordings were consistent with a pan-photoreceptor compromise with a cone>rod (CORD) pattern of retinal degeneration, which is consistent with the early-onset macular atrophic changes seen in all family members and the G pattern of field loss.

Genetic testing with next-generation exome sequencing (ES) revealed a heterozygous novel missense variant in the *TUBB4B* gene (c.784C>T, p.R262W; NM_006086.5; rs1836789108) (Fig. 1B), which segregated with disease in all of the proband's affected family members (except All2, who was unavailable for genetic testing) (Fig. 1A). This variant was classified as a variant of uncertain significance according to the American College of Medical Genetics and Genomics guidelines ¹⁹. It had not been previously published in the medical literature, is not observed in large population cohorts (gnomAD), and was predicted to be probably damaging by PolyPhen-2²⁰ (score 1.000) and deleterious by MutationTaster2025²¹ (score 101). Additional variants were also identified in patients AIII2 and AIII3; however, these variants did not segregate with disease in this family. Specifically, patient AIII2 harbored compound heterozygous variants in *ABCA4* (V931M *in trans* to R2107H) and compound heterozygous variants in *IFT140* (A686G *in trans* to A1238T). Patient AIII3 harbored a single heterozygous variant in *ABCA4* (R2107H).

Family B

A 56-year-old White British male (BII1) was first seen at Moorfields Eye Hospital at age

24 for evaluation of suspected bull's eye maculopathy. He reported longstanding difficulty with central vision, first noticing symptoms around the age of 13 when he began using glasses. He coped well with refractive correction until approximately age 19, when he experienced a noticeable decline in central visual acuity. Past medical history was notable for bilateral congenital ptosis, mild spina bifida, and childhood-onset post-lingual SNHL requiring hearing aids from the age of 5. There was no reported family history of visual or hearing impairment (Fig. 2A); both parents had normal hearing and vision throughout their lifetimes.

At his initial ophthalmic evaluation at age 24, his BCVA was 20/40 in each eye. At his most recent ophthalmic review at age 53, his visual acuity had deteriorated to counting fingers in the right eye and 20/1200 unaided in the left. Confrontation testing revealed full peripheral visual fields. Anterior segment examination showed mild lens opacities with good visualization of the fundus. Fundoscopy demonstrated widespread, symmetrical, well-demarcated macular atrophy with a relatively preserved surrounding retina (Fig. 2A). Peripheral retinal pigmentary changes and areas of atrophy were also noted. FAF imaging showed hypoautofluorescence centrally and in the periphery in each eye, corresponding to the areas of atrophy (Fig. 2B). Macular SD-OCT showed central retinal thinning in each eye (Fig. 2C). Electrophysiology testing performed at age 36 showed a cone-rod pattern of dystrophy with electronegative ERG (data not shown).

Genetic testing with whole genome sequencing identified only a single likely candidate variant, which was in the *TUBB4B* gene (c.784C>T, p.R262W; NM_006088.5).

Family C

A 42-year-old Chinese female (CIII6) initially presented to the Singapore National Eye Center for evaluation of poor vision since age 13 and childhood-onset pre-lingual SNHL with speech impediment. Her vision symptoms were nyctalopia and reduced vision, with BCVA of 1.6 logMAR (20/800 equivalent) in each eye on presentation. There was no reported family history of visual or hearing impairment (Fig. 2A). Slit lamp biomicroscopy examination of the anterior

segment revealed a dense combined cataract of the right eye. Dilated fundus evaluation (images shown were acquired at age 63 years) showed optic disc pallor, macular atrophy, dense bone spicule pigmentary deposits throughout the periphery, and pronounced vascular attenuation (Fig. 2A). FAF imaging showed nearly confluent hypoautofluorescence throughout the fundus, with hyperautofluorescent signal in central macula (Fig. 2B). Macular SD-OCT scans revealed severe outer retinal and RPE atrophy, retinal thinning, widespread HTDs, SHRM, severe attenuation of the choroid, and vitreomacular traction with subretinal fluid and intraretinal cysts (Fig. 2C). Retrospective review of patient's vision over the course of 20 years demonstrated a progressive decline in her BCVA to 3.0 logMAR (equivalent to no light perception, NLP) in each eye (Table 1).

Genetic testing with a Next Generation Sequencing identified a variant in the *TUBB4B* gene (c.784C>T, p.R262W; NM 006088.6).

DISCUSSION

Overview of known TUBB4B mutations

To date, the majority of reported mutations causing *TUBB4B*-associated retinopathies affect only two amino acid residues: R390 and R391. Patients with these mutations typically exhibit severe and early-onset photoreceptor dystrophy consistent with LCA, as well as hearing defects diagnosed between birth and 8 years of age. While most patients with amino acid substitutions at the R391 residue appear to exhibit a rod-cone dystrophy phenotype with vessel attenuation, pigmentary deposits, and degeneration in the mid-peripheral retina, patients with substitutions at the R390 residue show a distinctly pericentral pattern of degeneration ^{9-11, 13, 14}. In contrast to these rod-cone phenotypes, a recently reported K350T variant causes cone-rod dystrophy in addition to SNHL ²². All three variants are predicted to have negative effects on the stability of αβ-tubulin heterodimers, leading to diminished microtubule growth rates and impaired stability ^{9-11, 22}. Finally, a Y310H variant has also been reported to cause LCAEOD. However,

due to the young age of the patient, detailed ophthalmologic examination could not be performed; moreover, the molecular impact of this variant on TUBB4B function is unclear ¹¹. The cases reported herein presented with a cone-rod phenotype that shares similarities with the K350T manifestations reported by Scarpato et al. ²².

Several *TUBB4B* mutations result in retina-sparing systemic phenotypes. A recently reported *TUBB4B* mutation Q11R causes hearing loss, renal tubular Fanconi Syndrome, hypophosphatemic rickets, microphthalmia, and microcornea, but no retinal symptoms ⁷. A few mutations in *TUBB4B* (P259L, P259S, F242_R251dup) have been reported in individuals with primary ciliary dyskinesia (PCD), which is characterized by defects in motile cilia movement causing respiratory symptoms ²³. Additionally, a single variant, P358S, is reported to cause both PCD and LCAEOD, with some patients also exhibiting renal, heart or skeletal growth defects ²³. Finally, *TUBB4B* is also associated with determining handedness, as certain rare coding variants are linked to higher rates of left-handedness through an unknown mechanism ²⁴. It is unclear whether the R262W variant, reported herein, plays a role in determining handedness, as two (All1 and AllI3) of the six affected Family A members are left-handed, and the remaining four are right-handed. Information about the handedness of patients Bl11 and CllI6 is unavailable.

TUBB4B-associated phenotypes appear to be closely correlated with the molecular impact of each variant. For example, R390/R391 variants, which are exclusively associated with LCAEOD, destabilize interactions between heterodimers, increasing microtubule instability ^{11, 23}. In contrast, R259 variants, which are associated with PCD, disrupt heterodimerization thus inhibiting microtubule formation. Notably, these mechanisms act through a dominant negative effect rather than through haploinsufficiency, which is an important consideration for researchers seeking to develop treatments for these diseases. ²³

Proposed molecular impact of the TUBB4B R262W variant

The binding of kinesin motor proteins to microtubules is predominantly facilitated by

electrostatic interactions between the kinesin heavy chain and individual tubulin subunits. Specifically, several positively charged amino acids in the tubulin-binding region of kinesin associate closely with residues E410, D417, and E421 of the β-tubulin H12 helix (Figure 1C), which is conserved across nearly all β-tubulin isotypes ²⁵⁻²⁷. Although mutations affecting these key kinesin-binding residues have never been reported for TUBB4B, missense mutations at these positions in other β-tubulin isotypes are well documented to cause pathology ²⁸⁻³². Such mutations in the closely related TUBB3 gene cause fibrosis of the extraocular muscles (CFEOM) due to abnormal growth of cranial and central axons ^{15, 33}. Replacing any of these residues with alanine significantly reduces the affinity between kinesin and microtubules ²⁶. While the R262W variant, reported herein, is outside of the kinesin-binding domain of β-tubulin 4B, it may affect kinesin binding indirectly. The highly conserved residue R262 (Fig. S2A) is thought to form a hydrogen bond with D417, which is essential for properly positioning the H12 helix of β-tubulin to interact with kinesin¹⁵. Alternatively, AlphaFold3 modeling of β-tubulin 4B predicts an interaction between R262 and E421 (Fig. 1C), another key residue in the kinesinbinding domain. In TUBB3, R262C and R262H mutations cause phenotypes that are similar to those of the H12 helix mutations ¹⁵.

On the subcellular level, it remains to be determined which microtubule populations within photoreceptor cells are implicated in the pathophysiology of *TUBB4B*-associated retinopathies. Ciliary microtubules that form the axoneme facilitate indispensable molecular transport between the inner and outer segments, which may be impeded by the *TUBB4B* R262W variant. However, part of the pathology may also derive from the recently discovered microtubule-rich accessory inner segment (aIS). The aIS is a microtubule-based extension of the inner segment of human rods, which extends alongside the majority of the outer segment length ³⁴. While the function of the aIS is not yet established, it appears to provide structural support to the outer segment. Potential loss of the aIS-mediated support due to *TUBB4B* mutations may certainly contribute to their pathology.

Comparison of TUBB4B R262W to R262 mutations in other β-tubulin isotypes

While the pathogenic variants in TUBB3 have the most thoroughly characterized phenotypes among all β -tubulins, R262 mutations have also been reported in several other β -tubulin isotypes. R262H missense mutation in TUBB2A is reported to cause a severe neurological phenotype encompassing arthrogryposis multiplex congenita, brain abnormalities, and profound developmental delay 35 . The same pathogenic R262H variant in TUBB4A similarly causes severe global developmental delay, axial hypotonia with appendicular hypertonia, and swallowing difficulties 36 . In TUBB8, R262Q mutation causes impaired oocyte meiotic spindle assembly, resulting in female infertility 37 . Given the high degree of conservation of the kinesin-binding domain across β -tubulin isotypes 25 (Fig. S2B), disease phenotypes associated with R262 mutations in TUBB2A, TUBB3, TUBB4A, and TUBB8 support the presumed pathogenicity of the novel R262W variant in TUBB4B.

Notably, R262 mutations in other β -tubulins do not result in retinal phenotypes, which is likely explained by the unique β -tubulin expression profiles across different tissues and cell types. Although many non-photoreceptor cell types in the retina express combinations of multiple β -tubulins, the only β -tubulin isotype appreciably expressed in photoreceptor cells (both rods and cones) is TUBB4B (Fig. 5) $^{38, 39}$. Therefore, mutations in TUBB4B are expected to produce a greater impact in photoreceptors compared to cell types wherein β -tubulin 4B is not the overwhelmingly predominant isotype. Although TUBB4B is ubiquitously expressed in human tissues, including throughout the neuroretina, RPE, and the choroid, the presence of additional β -tubulin isotypes in other tissues likely mitigates the negative impact of the R262 mutation.

In conclusion, this report advances our understanding of *TUBB4B*-associated retinopathies by expanding their mutation spectrum outside of the canonical R390/R391 hotspot, as well as by broadening their range of clinical manifestation beyond the early-onset phenotype of LCA.

FIGURES

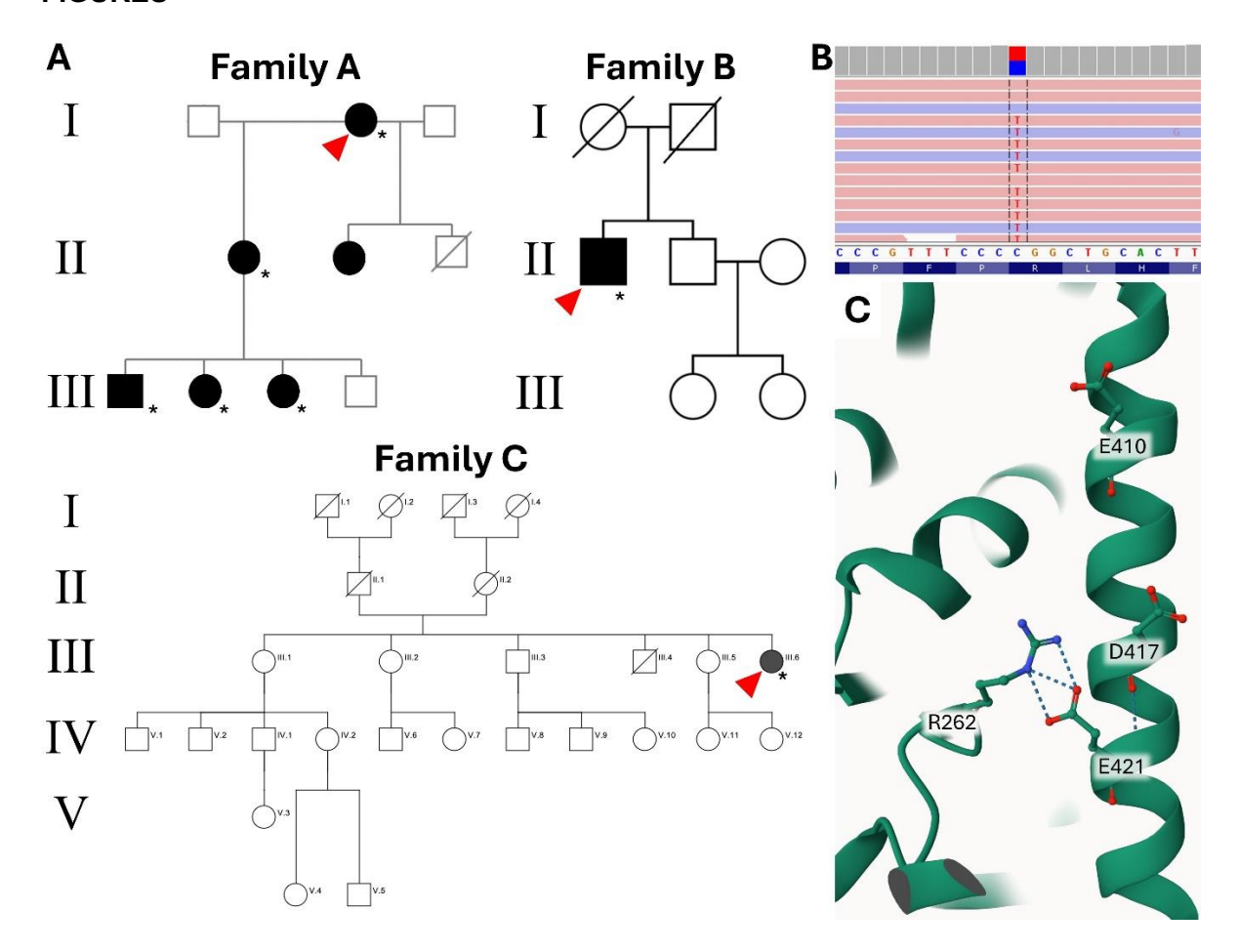


Figure 1. Genetic and molecular characteristics of the *TUBB4B* c.784C>T (p.R262W) variant. (A) Pedigrees of the three examined families. Red arrowhead indicates the proband; * indicates presence of molecularly confirmed *TUBB4B* variant. Individuals AI1, AI3, AII2, and AIII4 were unavailable for genetic testing. The local family identifier of Family B is GC16775. (B) Next generation sequencing (NGS) demonstrated the presence of heterozygous *TUBB4B* variant c.784C>T (p.R262W) in all affected Family A members (except AII2, who was unavailable for genetic testing). Only the proband's result is shown. Colors in the NGS read: red – thymine (T); blue – cytosine (C). Sequencing data for Families B and C are not shown. (C) Protein ribbon structure of the kinesin-binding domain of β-tubulin 4B chain, generated by AlphaFold3, demonstrates the location of residue R626 and its predicted interaction with residue E421. ¹⁸

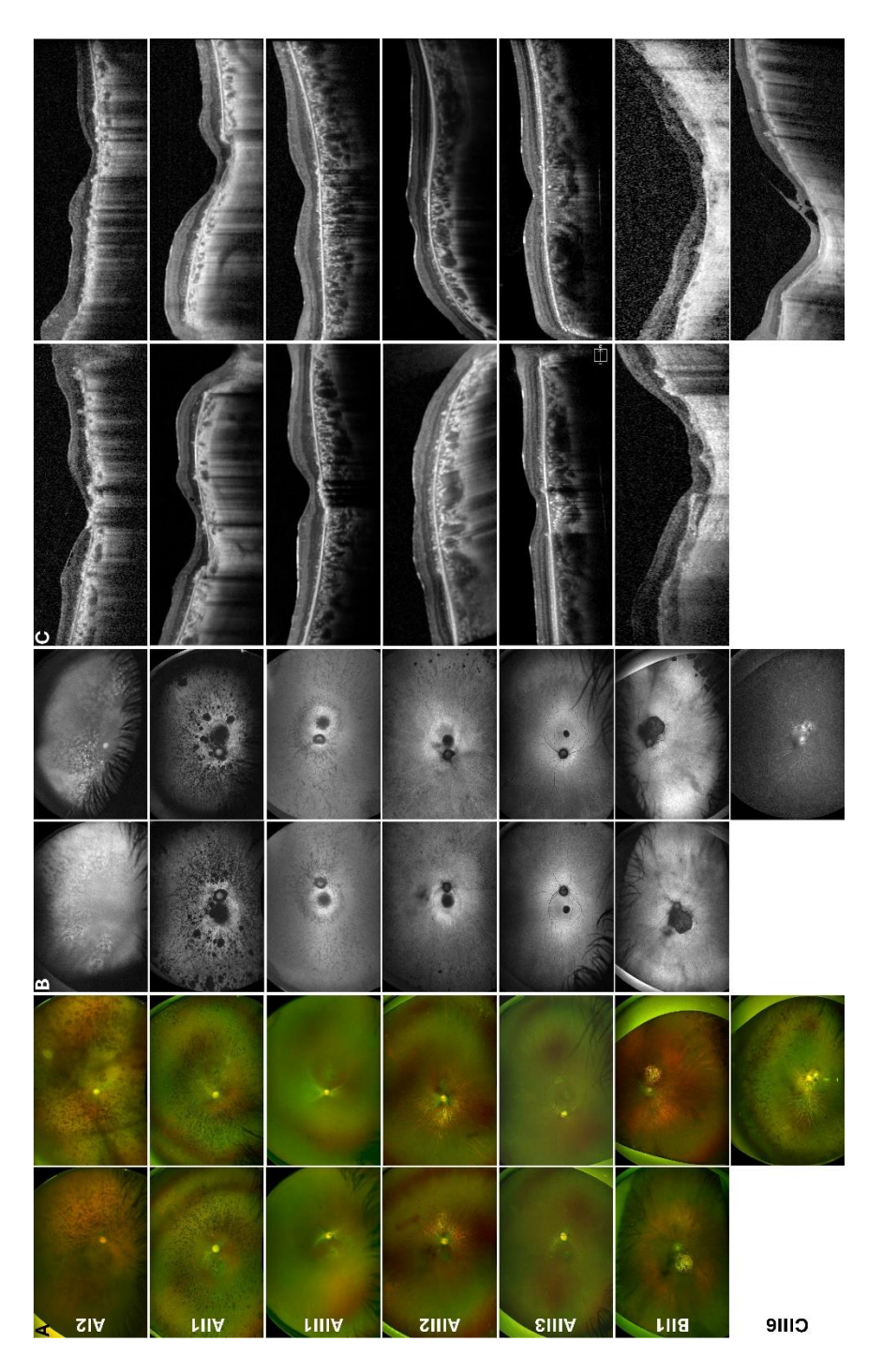


Figure 2. Retinal imaging, including ultra-widefield pseudocolor fundus photographs **(A)**, fundus autofluorescence photographs **(B)**, and spectral-domain optical coherence tomography (SD-OCT) scans through the foveola **(C)** of all examined patients. Views of the fundi were partially obstructed by bilateral cataracts in patient Al2 and completely obstructed by right eye cataract in patient CIII6.

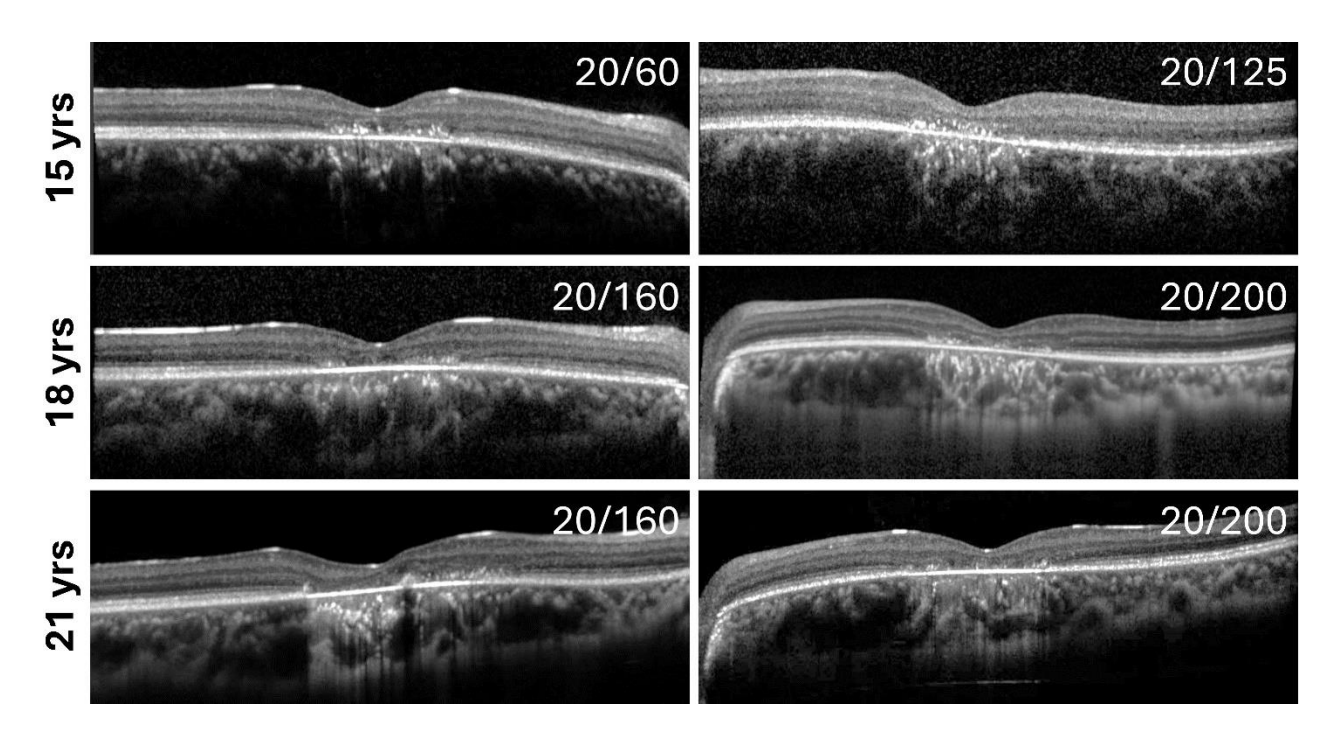


Figure 3. Progression of subfoveal outer retinal atrophy in patient AIII3. Sequential SD-OCT scans through the foveola were obtained over the period of six years at the indicated ages. The corresponding ETDRS visual acuities are indicated.

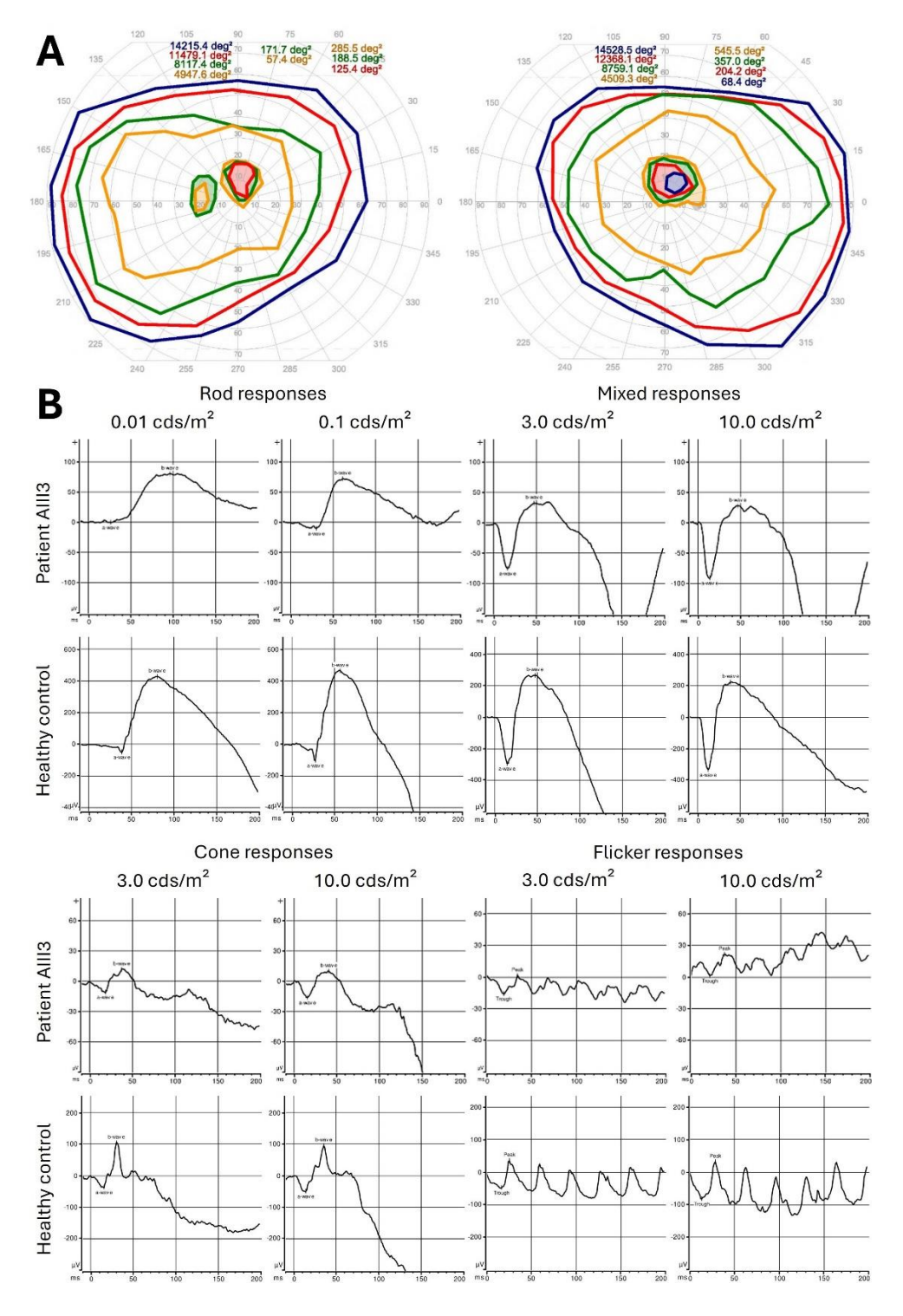


Figure 4. Functional assessment of the retina of patient AIII3. **(A)** Goldmann kinetic perimetry of both eyes was performed with the following stimulus sizes: I3e (orange), I4e (green), III4e (red), V4e (blue). **(B)** Full-field ERG recordings from the right eye of patient AIII3 and a healthy agematched control. Left eye recordings (not shown) were similar.

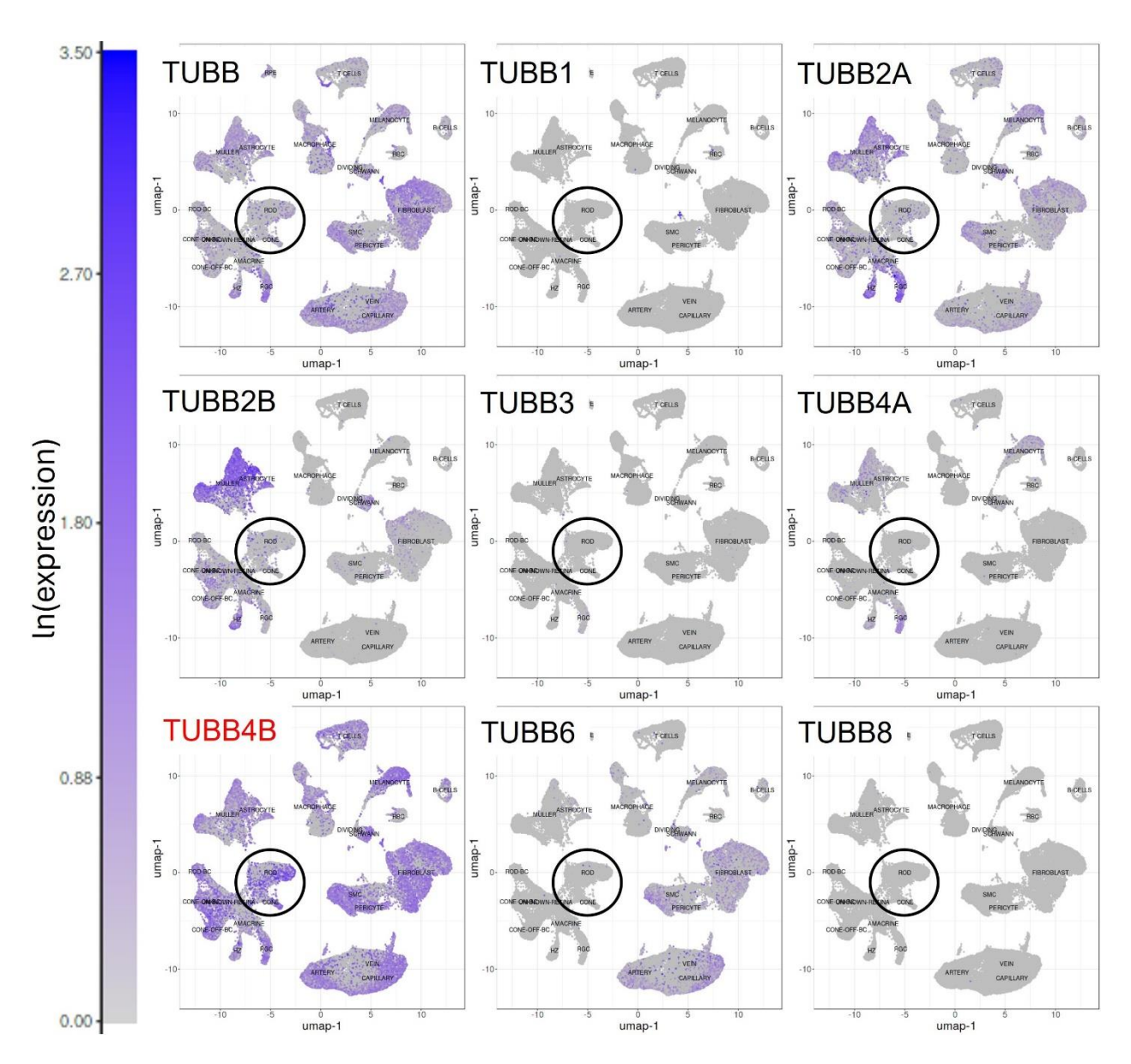


Figure 5. *TUBB4B* is expressed throughout the neuroretina, RPE, and the choroid, with marked enrichment in rod and cone photoreceptors compared to other β-tubulin isotypes. Single-cell RNA sequencing analysis was generated by Spectacle based on the integrated lowa dataset. Deeper shades of blue indicate higher transcript expression levels, on a natural log scale as indicated on the left. Rod and cone photoreceptor cluster is indicated with black circles.

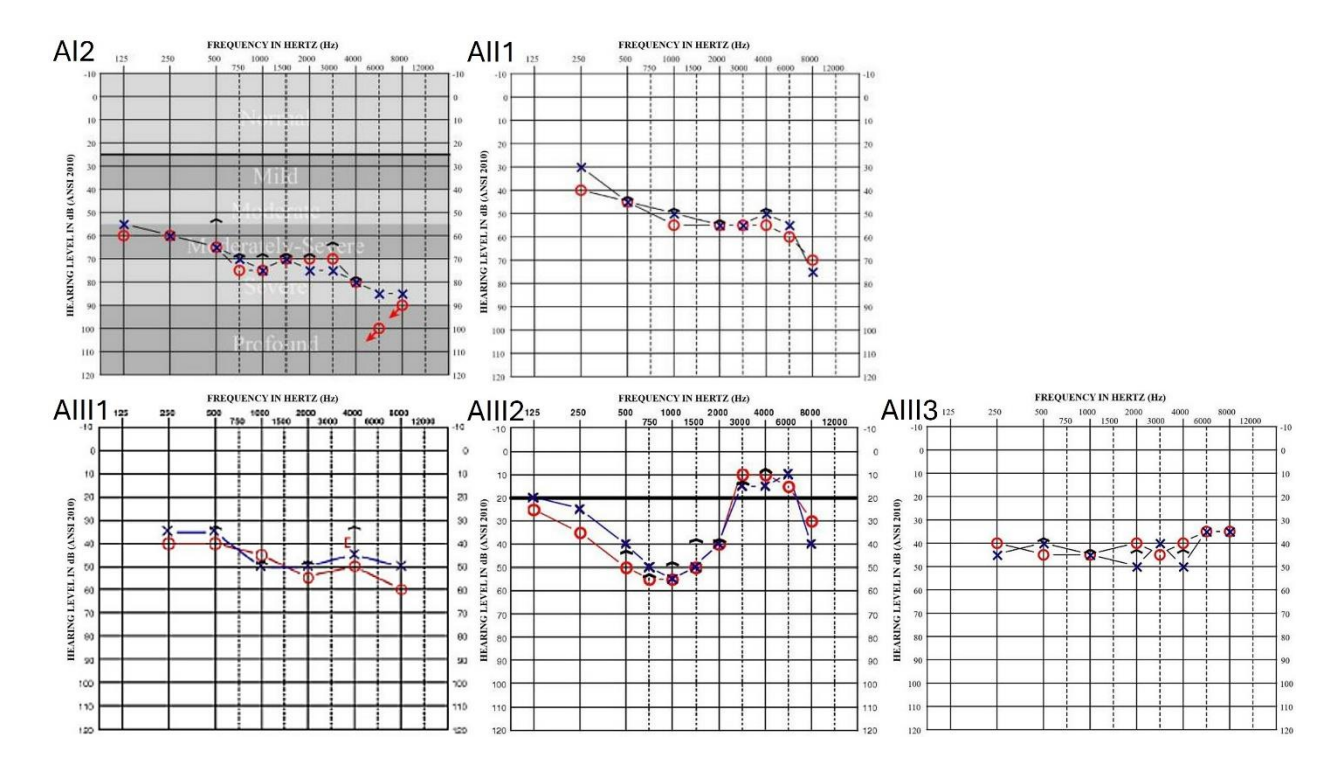


Figure S1. Audiograms of all examined Family A members revealed bilaterally symmetrical SNHL, the severity of which appears to generally correlate with age. Hearing thresholds (dB) measured with unmasked air conduction from the right (red circle) and left (blue cross) ear are plotted at the indicated range of sound frequencies (Hz).

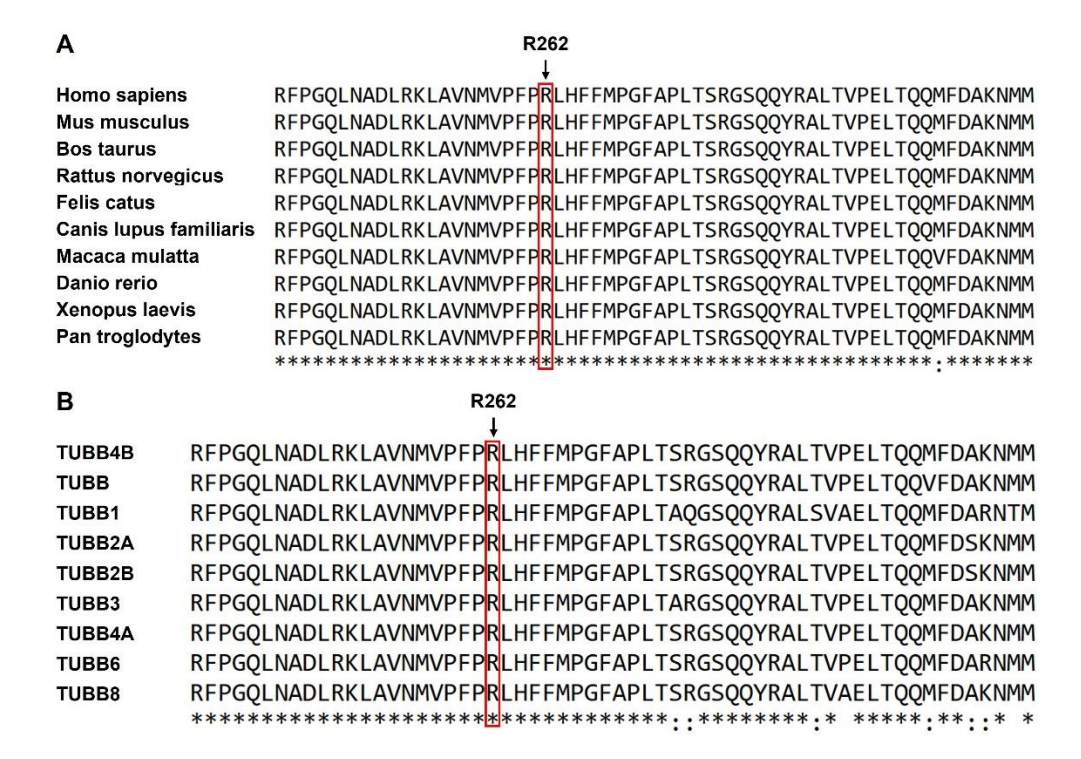


Figure S2. The R262 residue is highly conserved across TUBB4B vertebrate orthologues (**A**) and across the other human β-tubulin isotypes (**B**). Alignments were performed using Clustal Omega. "*" indicates positions with fully conserved residues; ":" indicates positions with strong conservation.

Age (years)	Right eye BCVA (logMAR)	Left eye BCVA (logMAR)
42	1.6	1.6
43	1.6	2.3
44.5	1.6	2.7
46	2.7	2.7
50	2.7	2.7
51.2	2.7	2.7
61.75	3.0	3.0

Table 1. Progression of BCVA deterioration in patient CIII6. ETDRS visual acuity was measured in each eye over the course of 20 years at the indicated ages. Off-chart visual acuities were converted to logMAR equivalents (logMAR 2.3, hand motions; 2.7, light perception; 3.0, no light perception).

AUTHOR CONTRIBUTIONS STATEMENT

Conception and design: OA

Data analysis and interpretation: LYC, AD, EHJ, RSM, SR, ERS, OAM, ARW, SL, BJF, AI, OA

Drafting of the manuscript: LYC, EHJ, SL, BJF, OA

Critical revision of the manuscript: LYC, AD, EHJ, RSM, SR, ERS, OAM, ARW, SL, BJF, AI, OA Final approval of the version to be published: LYC, AD, EHJ, RSM, SR, ERS, OAM, ARW, SL,

BJF, AI, OA

All authors agree to be accountable for all aspects of the work.

DISCLOSURE STATEMENT

SR is an employee of and may hold stock in GeneDx, LLC

FUNDING

This work was supported by the Foundation Fighting Blindness Career Development Award (RSM), Wellcome Trust 206619/Z/17/Z (OAM), Fight for Sight UK (OAM), Retina UK (OAM), (OAM), MRC Clinician Scientist Fellowship UKRI440 (SL), NIHR Manchester Biomedical Research Centre (BRC) NIHR203308 (SL), SingHealth Foundation (BJF), National Eye Institute grant EY033857 (OA) and Duke University Physician-Scientist Strong Start Award (OA).

REFERENCES

- 1. Chandra B, Tung ML, Hsu Y, Scheetz T, Sheffield VC. Retinal ciliopathies through the lens of Bardet-Biedl Syndrome: Past, present and future. *Prog Retin Eye Res* 2022;89:101035.
- 2. Pearring JN, Salinas RY, Baker SA, Arshavsky VY. Protein sorting, targeting and trafficking in photoreceptor cells. *Prog Retin Eye Res* 2013;36:24-51.
- 3. Cushion TD, Leca I, Keays DA. MAPping tubulin mutations. *Front Cell Dev Biol* 2023;11:1136699.
- 4. Alberts B. *Molecular biology of the cell*. 4th ed. New York: Garland Science; 2002:xxxiv, 1548 p.
- 5. Roll-Mecak A. The Tubulin Code in Microtubule Dynamics and Information Encoding. *Dev Cell* 2020;54:7-20.
- 6. Bahi-Buisson N, Maillard C. Tubulinopathies Overview. In: Adam MP, Feldman J, Mirzaa GM, Pagon RA, Wallace SE, Amemiya A (eds), *GeneReviews*. Seattle (WA): University of Washington; 1993.
- 7. McFadden JR, Tolete CDP, Huang Y, et al. Clinical, genetic, and structural characterization of a novel TUBB4B tubulinopathy. *Mol Genet Metab Rep* 2023;36:100990.
- 8. Gomes NL, Greenstein VC, Carlson JN, et al. A comparison of fundus autofluorescence and retinal structure in patients with Stargardt disease. *Invest Ophthalmol Vis Sci* 2009;50:3953-3959.
- 9. Luscan R, Mechaussier S, Paul A, et al. Mutations in TUBB4B Cause a Distinctive Sensorineural Disease. *Am J Hum Genet* 2017;101:1006-1012.
- 10. Maasz A, Hadzsiev K, Ripszam R, et al. TUBB4B gene mutation in Leber phenotype of congenital amaurosis syndrome associated with early-onset deafness. *Eur J Med Genet* 2022;65:104471.
- 11. Bodenbender JP, Marino V, Philipp J, et al. Comprehensive analysis of two hotspot codons in the TUBB4B gene and associated phenotypes. *Sci Rep* 2024;14:10551.
- 12. Gregory-Evans CY, Joe AW, Gregory-Evans K. Mutation of beta-tubulin 4B gene (TUBB4B) causes autosomal dominant retinitis pigmentosa with sensorineural hearing loss in a multigenerational family. *Mol Vis* 2025;31:175-188.
- 13. Medina G, Perry J, Oza A, Kenna M. Hiding in plain sight: genetic deaf-blindness is not always Usher syndrome. *Cold Spring Harb Mol Case Stud* 2021;7.
- 14. Long YL, Liu X, Wang G, Liu B, Meng XH, Liu Y. The first Chinese case with LCAEOD syndrome caused by mutation of TUBB4B gene. *Int J Ophthalmol* 2025;18:753-756.
- 15. Tischfield MA, Baris HN, Wu C, et al. Human TUBB3 mutations perturb microtubule dynamics, kinesin interactions, and axon guidance. *Cell* 2010;140:74-87.
- 16. Retterer K, Juusola J, Cho MT, et al. Clinical application of whole-exome sequencing across clinical indications. *Genet Med* 2016;18:696-704.
- 17. Martin AR, Williams E, Foulger RE, et al. PanelApp crowdsources expert knowledge to establish consensus diagnostic gene panels. *Nature genetics* 2019;51:1560-1565.
- 18. Abramson J, Adler J, Dunger J, et al. Accurate structure prediction of biomolecular interactions with AlphaFold 3. *Nature* 2024;630:493-500.
- 19. Richards S, Aziz N, Bale S, et al. Standards and guidelines for the interpretation of sequence variants: a joint consensus recommendation of the American College of Medical Genetics and Genomics and the Association for Molecular Pathology. *Genet Med* 2015;17:405-424.
- 20. Adzhubei IA, Schmidt S, Peshkin L, et al. A method and server for predicting damaging missense mutations. *Nat Methods* 2010;7:248-249.

- 21. Steinhaus R, Proft S, Schuelke M, Cooper DN, Schwarz JM, Seelow D. MutationTaster2021. *Nucleic Acids Res* 2021;49:W446-w451.
- 22. Scarpato M, Testa F, Nesti A, et al. A Novel Variant in TUBB4B Causes Progressive Cone-Rod Dystrophy and Early Onset Sensorineural Hearing Loss. *Mol Genet Genomic Med* 2025;13:e70068.
- 23. Dodd DO, Mechaussier S, Yeyati PL, et al. Ciliopathy patient variants reveal organelle-specific functions for TUBB4B in axonemal microtubules. *Science* 2024;384:eadf5489.
- 24. Schijven D, Soheili-Nezhad S, Fisher SE, Francks C. Exome-wide analysis implicates rare protein-altering variants in human handedness. *Nat Commun* 2024;15:2632.
- 25. Hausrat TJ, Radwitz J, Lombino FL, Breiden P, Kneussel M. Alpha- and beta-tubulin isotypes are differentially expressed during brain development. *Dev Neurobiol* 2021;81:333-350.
- 26. Uchimura S, Oguchi Y, Katsuki M, et al. Identification of a strong binding site for kinesin on the microtubule using mutant analysis of tubulin. *EMBO J* 2006;25:5932-5941.
- 27. Cao L, Wang W, Jiang Q, Wang C, Knossow M, Gigant B. The structure of apo-kinesin bound to tubulin links the nucleotide cycle to movement. *Nat Commun* 2014;5:5364.
- 28. Niwa S, Takahashi H, Hirokawa N. beta-Tubulin mutations that cause severe neuropathies disrupt axonal transport. *EMBO J* 2013;32:1352-1364.
- 29. Cai S, Li J, Wu Y, Jiang Y. De novo mutations of TUBB2A cause infantile-onset epilepsy and developmental delay. *J Hum Genet* 2020;65:601-608.
- 30. Sferra A, Fattori F, Rizza T, et al. Defective kinesin binding of TUBB2A causes progressive spastic ataxia syndrome resembling sacsinopathy. *Hum Mol Genet* 2018;27:1892-1904.
- 31. Chew S, Balasubramanian R, Chan WM, et al. A novel syndrome caused by the E410K amino acid substitution in the neuronal beta-tubulin isotype 3. *Brain* 2013;136:522-535.
- 32. Cederquist GY, Luchniak A, Tischfield MA, et al. An inherited TUBB2B mutation alters a kinesin-binding site and causes polymicrogyria, CFEOM and axon dysinnervation. *Hum Mol Genet* 2012;21:5484-5499.
- 33. Puri D, Barry BJ, Engle EC. TUBB3 and KIF21A in neurodevelopment and disease. *Front Neurosci* 2023;17:1226181.
- 34. Lewis TR, Klementieva NV, Phan S, Castillo CM, Kim KY, Cao LY, Ellisman MH, Arshavsky VY, Alekseev O. Unique ultrastructural organization of human rod photoreceptors. *Commun Biol.* 2025;8:63.
- 35. Ejaz R, Lionel AC, Blaser S, et al. De novo pathogenic variant in TUBB2A presenting with arthrogryposis multiplex congenita, brain abnormalities, and severe developmental delay. *Am J Med Genet A* 2017;173:2725-2730.
- 36. Ferreira C, Poretti A, Cohen J, Hamosh A, Naidu S. Novel TUBB4A mutations and expansion of the neuroimaging phenotype of hypomyelination with atrophy of the basal ganglia and cerebellum (H-ABC). *Am J Med Genet A* 2014;164A:1802-1807.
- 37. Feng R, Sang Q, Kuang Y, et al. Mutations in TUBB8 and Human Oocyte Meiotic Arrest. *N Engl J Med* 2016;374:223-232.
- 38. Voigt AP, Whitmore SS, Lessing ND, et al. Spectacle: An interactive resource for ocular single-cell RNA sequencing data analysis. *Exp Eye Res* 2020;200:108204.
- 39. Voigt AP, Whitmore SS, Flamme-Wiese MJ, et al. Molecular characterization of foveal versus peripheral human retina by single-cell RNA sequencing. *Exp Eye Res* 2019;184:234-242.